Scattering-theoretic approach to elastic one-electron tunneling through localized barriers: Application to scanning tunneling microscopy

A. A. Lucas,* H. Morawitz, and G. R. Henry

IBM Almaden Research Center, 650 Harry Road, San Jose, California 95120-6099

J.-P. Vigneron and Ph. Lambin

Facultes N.-D. de la Paix, 61 rue de Bruxelles, B-5000, Namur, Belgium

P. H. Cutler and T. E. Feuchtwang

Pennsylvania State University, 104 Davey Laboratory, University Park, Pennsylvania 16802

A new formulation of elastic one-electron tunneling through three-dimensional (3D), nonseparable, spatially localized barriers is developed in terms of potential-scattering theory. To illustrate the principles of the method, a model metal-vacuum-metal junction is used, consisting of two parallel electrodes, one of which has a hemispherical protrusion. The electronic structure of each metal electrode is assumed to be free-electron-like, for simplicity. The bias and multiple-image tunneling barriers for this model are constructed on the basis of classical electrostatics and a simple quantum correction at the metal surfaces. Regarding the barrier as made of a planar, separable part plus a nonseparable, localized perturbation due to the spherical boss, the exact, unperturbed, one-electron Green's function of the planar part is first obtained by numerical integration of the corresponding, effectively 1D Schrödinger equation. Then the localized boss potential is treated to all orders of perturbation by solving the Dyson equation for the full barrier Green's function, using a real-space discretization of the integral equation on a finite grid. New useful formulas are derived for correcting the discretization error associated with ignoring the singular diagonal matrix elements of the Green's functions. The tunneling current density is then expressed in terms of the exact 3D wave functions which are obtained at the grid points by discretizing the Lippmann-Schwinger equation. The axial symmetry of the present barrier model leads to a reduction of the size of the Green's matrices, since the wave functions of different axial angular momenta contribute independently to the tunneling. The $m = 0$ wave functions are found to contribute 90% of the total tunnel current at the Fermi level. The new method is applied to a discussion of the lateral resolution of the scanning tunneling microscope. It is found that the current distribution peaks within a narrow angle around the boss axis, confirming earlier estimates based on the transfer-Hamiltonian formalism and in agreement with the observed atomic resolution of the microscope, when operating with atomic-size tips. The present Green's-function method is applicable to several other problems of one-electron tunneling through localized barriers and may be extended to incorporate such effects as the corrugation and the band structure of the electrodes. Moreover, the method lends itself to a quantitative assessment of the accuracy of approximate tunneling theories such as the transfer-Hamiltonian formalism when applied to elastic one-electron tunneling problems.

I. INTRODUCTION

As discussed in the classic review by Duke,[1] tunneling problems have been traditionally treated either with the Oppenheimer-Bardeen transfer-Hamiltonian method,[2,3] or by evaluating current-carrying eigenstates of a one-electron model Hamiltonian. While the former method is approximate and restricted to weakly coupled electrodes, the latter is, in principle, exact for independent-electron systems. However, up to now the model-Hamiltonian method has been applied mainly to separable Hamiltonians, i.e., to situations which can effectively be reduced to a one-dimensional Schrödinger problem through exploitation of the translational or other symmetries of the tunnel barrier. By and large, tunneling through three-

dimensional (3D) barriers has been approached mostly by the transfer-Hamiltonian method.

Recently, a more complete many-body theory of tunneling going beyond the transfer-Hamiltonian formalism has been developed based on Keldysh's theory of nonequilibrium processes.[4] However, to our knowledge, the theory has so far remained at the formal stage since, in practice, no tunneling calculation has been done with it.

The recent development of scanning tunneling microscopy (STM) and spectroscopy[5] has dramatized the need for an accurate and feasible 3D tunneling theory. This is because the atomic resolution of STM implies that the tunneling action proceeds from a microscopic, perhaps single-atom, metallic tip through a highly inhomogeneous barrier. Since the radius of curvature of the STM tip is of

the order of the metal Fermi wavelength, one cannot ignore the 3D aspect of this barrier. Indeed, it is by virtue of its high lateral inhomogeneity that the atomic resolution of the microscope is obtained. Thus, the transfer-Hamiltonian approach has so far been the method of choice for interpreting the micrographs and other properties observed by STM.[6,7] One exception is the recent theoretical work of Stoll et al.,[8] who were able to treat a model-Hamiltonian–type barrier having a periodic, one-dimensional corrugation through the use of potential-scattering theory.

Typical current intensities in STM are in the nA range, under biases of a few meV only. It is straightforward to estimate that such currents passing through small clusters of atoms imply an unusually high rate of successful tunneling attempts by electrons close to the Fermi level impinging onto the barrier. One may then ask to what extent a weak-coupling theory such as the transfer-Hamiltonian theory remains adequate in such a situation. The purpose of the present paper is to develop a new approach to the model-Hamiltonian method which allows one to calculate elastic one-electron tunneling currents, in principle, exactly even in the strong-coupling case. It therefore should help in assessing the accuracy of the widely used transfer-Hamiltonian technique as well as other approximation methods.

The new method to be described applies to localized, nonseparable barriers. By localized, we mean situations in which nonperiodic spatial variations of barrier height and thickness occur over distances not much larger than the Fermi wavelength of the electrons. This is precisely the case of STM, but several other tunneling problems are of this category as well, such as, for example, the field ionization of imaging gas atoms in field-ion microscopy or the two-step tunneling through impurity states in metal-insulator-metal (M-I-M) junctions, etc.

The basic ideas of the proposed method are as follows. The tunneling problem is regarded as a problem in potential-scattering theory. The current density, which is a sum of expectation values of the current operator with respect to tunneling wave functions, is determined by calculating the scattering of wave functions incident on the barrier potential. The total barrier is split into an unperturbed part [for example, a planar metal-vacuum-metal (MVM) barrier in STM] and a perturbation localized in a small region of space where most of the tunneling current occurs. The unperturbed part is assumed to be an exactly soluble problem by virtue of the separability of its Hamiltonian in some coordinate system. Then the unperturbed wave functions, together with the known localized perturbation barrier, can be used to first construct the full Green's function of the total tunneling Hamiltonian via the Dyson equation and, secondly, the exact tunneling wave functions via the Lippmann-Schwinger equation. The crucial feature which makes this scheme feasible is the localized nature of the perturbation. Because of this, both the Dyson and the Lippmann-Schwinger integral equations can be discretized on a grid of a finite number of points covering only the spatial region where the barrier perturbation does not vanish. The integral equations for tunneling are thus transformed into simple matrix equations easily handled on the computer. The method represents, to our knowledge, the first application to a tunneling problem of the localized Green's-function technique extensively used in the study of the electronic structure of point defects in semiconductors.[9]

In Sec. II the tunnel barrier is constructed for a model MVM junction representative of the STM situation. It is made of two parallel, semi-infinite free-electron metals, on one of which is embedded a hemispherical protrusion. One reason for considering this geometry is that both its static-bias potential distribution and the all-important, multiple-image contribution to the tunneling barrier in the vacuum region can be given a simple classical representation.[10,11] The choice of working with free electrons is dictated by our desire to test the feasibility of the general approach on the simplest possible electronic structure of the electrodes. We outline, in Sec. III, the scattering-theoretic method. Section IV is devoted to the discretization scheme and to developing an important correction formula which takes account of the effect associated with the singularity of the diagonal matrix elements of the Green's functions. In Sec. V we solve the planar tunneling problem. In Sec. VI we show how the dimensions of the Green's matrices are reduced by exploiting the axial symmetry of the barrier model. In Sec. VII we present numerical results for the tunnel current density and its relationship to the lateral resolution of STM; we also discuss possible improvements of the model for this particular application. Finally, in Sec. VIII we briefly indicate other possible applications of the new method and also consider its future use for testing the accuracy of approximate one-electron tunneling theories.

II. BARRIER MODEL

The geometry of the tunnel junction is shown in Fig. 1(a). The electrodes are free-electron metals separated by a distance D in vacuum. The left-hand electrode ($z < 0$) has a hemispherical protrusion of radius R. A hemisphere is chosen for simplicity of construction of the multiple-image contribution to the tunnel barrier in the region of the boss as discussed below.[10,11]

The potential barrier $V(\mathbf{r})$ is decomposed into a planar, translationally invariant part $V_p(z)$, valid far away from the boss, and a nonseparable perturbation $V_{\text{loc}}(\mathbf{r})$ due to the boss, as illustrated symbolically in Fig. 1(b):

$$V(\mathbf{r}) = V_p(z) + V_{\text{loc}}(\mathbf{r}) \ . \tag{1}$$

The perturbation V_{loc} is not small but is localized, an essential requirement in our subsequent application of the Green's-function technique for scattering by localized perturbations.[9]

A. The planar barrier

The planar barrier has two terms,

$$V_p(z) = V_{\text{bias}}(z) + V_{\text{im}}(z) \ , \tag{2}$$

where V_{bias} is the external bias potential and V_{im} is the electron image potential. $V_{\text{bias}}(z)$ is linear in the vacuum

(a)

(b)
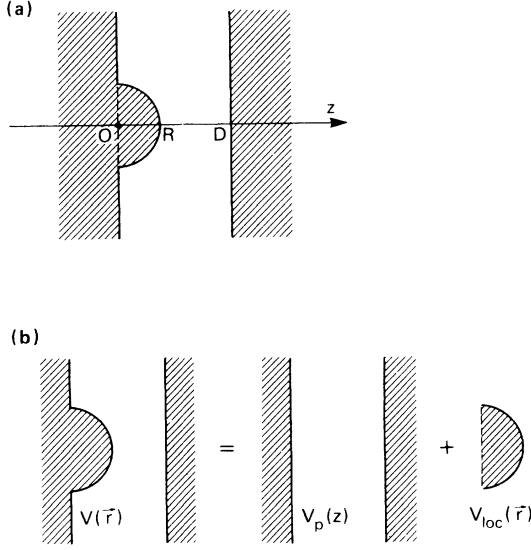
FIG. 1. (a) Plane-spherical geometry of the model STM junction. (b) Symbolic decomposition of the total tunnel barrier into a planar part and a localized part.

$$V_{im}(z) = \frac{e^2}{2} \int_0^{k_c} dk \frac{\beta^2}{1 - \beta^2 e^{-2kD}}$$

$$\times \left[2e^{-2kD} - \frac{1}{\beta}(e^{-2k(D-z)} + e^{-2kz}) \right],$$

(3)

where $\beta = (\epsilon - 1)/(\epsilon + 1)$ is the familiar surface screening factor involving the static dielectric constant of the materials ($\beta = 1$ for metals). The classical divergence at $z = 0$ and $z = D$ of the normally infinite integral has been removed by introducing a cutoff wave vector k_c. This cutoff is imposed by the physical requirement that the Fourier components of the surface screening charge density have wavelengths no shorter than the mean valence-electron separation in the material. The surface value of the image potential is then $-e^2 k_c / 2$ and can be adjusted, through k_c, so as to join continuously to the inner potential V_{in} of the metal. Alternatively, we can expand the denominator in Eq. (3) in powers and integrate term by term to generate the multiple-image series of the method of images. The divergence at $z = 0$, D, of the first-order image potential can then be eliminated by applying the simple quantum correction prescribed by Seitz,[12] i.e., by withdrawing the image plane inside the metal by an amount z_0. z_0 is again adjusted to join continuously to V_{in}. The result is (for $\beta = 1$)

region and is constant within the metal electrodes beyond a small field-penetration distance which we shall take equal to zero. Solving Poisson's equation leads to the simple representation of V_{im} in vacuum as follows:

$$V_{im}(z) = \frac{e^2}{4} \left[\frac{2}{D} - \frac{1}{D + z_0 - z} - \frac{1}{z_0 + z} \right] + \frac{e^2}{4} \sum_{n=1}^{\infty} \left[\frac{2}{(n+1)D} - \frac{1}{(n+1)D - z} - \frac{1}{nD + z} \right].$$

(4)

The two formulas (3) and (4) give very close results. A more refined approach for constructing V_{im} has recently been given in Ref. 13 in a form identical to our Eq. (3) above, but with $k_c = \infty$ and

$$\beta = [2\xi(\xi + k/k_T) - 1]^{-1}, \quad \xi = (1 + k^2/k_T^2)^{1/2}$$

(5)

where k_T is the Thomas-Fermi wave vector. We have checked that this approach does not differ from Eq. (3) or (4) by more than a few percent if k_T is adjusted to the same boundary condition of joining to V_{in}. In our work, we have used Eq. (4) because the method of images is easily implemented in the presence of the hemispherical protrusion, whereas a formula generalizing (3) to this geometry is not known.

B. The localized barrier

The principal perturbation effect of the boss is to substitute a constant inner potential V_{in} to the planar barrier compound above within the hemispherical region occupied by the boss. In addition, in the remaining vacuum gap around the boss, the bias, and multiple-image contributions are also modified. We can thus write

$$V_{loc}(\mathbf{r}) = V_{in}(\mathbf{r}) + V_{out}(\mathbf{r}),$$

(6)

where, inside the boss,

$$V_{in}(\mathbf{r}) = [V_{in} - V_p(z)]\Theta(\mathbf{r} - \mathbf{r}_{boss}),$$

(7)

whereas, within the vacuum gap,

$$V_{out}(\mathbf{r}) = [V_{bias}(\mathbf{r}) + V_{im}(\mathbf{r})][1 - \Theta(\mathbf{r} - \mathbf{r}_{boss})],$$

(8)

where Θ is the Heaviside step function and where $V_{bias}(\mathbf{r})$ and $V_{im}(\mathbf{r})$ have been computed in Ref. 10. Explicitly, $V_{bias}(\mathbf{r})$ is given by Eqs. (13) and (14) of the first of Ref. 10, whereas $V_{im}(\mathbf{r})$ is given by Eq. (16), from which the planar image result $V_{im}(z)$ must be subtracted out since, in the boss region, this term is already included in the total barrier of Eq. (1) above. Note that Eq. (16) of Ref. 10 must be corrected by applying Seitz's prescription to the first-order images in order for this formula to coincide with our Eq. (4) above at large distance from the boss.

The overall tunneling barrier so constructed is represented in Fig. 2 for zero bias and for the indicated
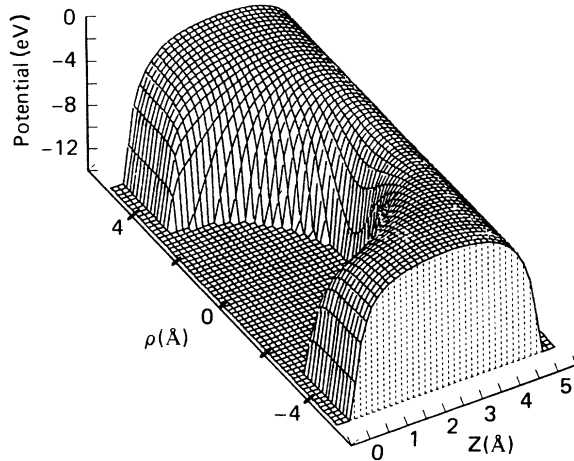
FIG. 2. The 3D tunneling barrier of the junction of Fig. 1 for $D = 5$ Å and $R = 3$ Å and for zero bias. The metal inner potential is -14 eV. The Fermi level used was at -4.5 eV.

values of the material and geometrical parameters. Note that one could eliminate the cusps at the metal surfaces by introducing a smooth joining of the vacuum barrier to V_{in}. This, however, is unnecessary at this stage in view of the coarseness of the grid that we shall use to sample the barrier in our discretization scheme of the scattering equations.

The highly inhomogeneous and localized nature of the image-dominated tunnel barrier (Fig. 2 is for zero bias) is evident. While it is obvious that the tunnel current will pass predominantly through the thinner and lower axial region of the barrier, it is impossible to reliably predict how the current density will decrease away from this region without a full 3D tunneling calculation.

III. INTEGRAL EQUATIONS FOR TUNNELING

Tunneling through the potential barrier of Eq. (1) will now be described as a problem in scattering theory. We envisage electron waves impinging onto the barrier and being partly transmitted through it. In the present paper we will consider only forward bias and zero temperature, so that tunneling proceeds only from left to right (Fig. 2). Our boundary condition for the scattering problem is then one of plane-wave states $| \mathbf{k} \rangle$ of energy E below the top of the barrier being incident from the left ($z < 0$) and being reflected and transmitted by the barrier.

We begin by writing the Lippmann-Schwinger equation for the state scattered by the planar barrier $V_p(z)$ alone as

$$| \phi_k \rangle = (1 + gV_p) | \mathbf{k} \rangle , \qquad (9)$$

where g is the Green's operator for energy E appropriate to the planar problem. The $\mathbf{r}$ representation of g and of $| \phi_k \rangle$ can be calculated to any desired accuracy due to the translational invariance of V_p and the consequent separability of this problem.

Once the unperturbed planar state $| \phi_k \rangle$ is known, we

can write the Lippmann-Schwinger equation for the exact state $| \psi_k \rangle$ scattered by the total barrier $V(\mathbf{r})$ as

$$| \psi_k \rangle = (1 + GV_{loc}) | \phi_k \rangle , \qquad (10)$$

where G is now the Green's operator at energy E for the 3D barrier. The planar and full Green's operators are related through the Dyson equation

$$G = (1 - gV_{loc})^{-1}g . \qquad (11)$$

Hence, in principle, we can construct G and $| \psi_k \rangle$ from the knowledge of the planar solution $| \phi_k \rangle$ and g, together with the localized perturbation V_{loc}.

We are interested in obtaining the total current density associated with all plane waves incident on the barrier from the left, especially in the region of the planar electrode immediately facing the boss (Fig. 3). Indeed, this is the key quantity for appreciating the inhomogeneity and anisotropy of the tunneling and hence the lateral resolution of this STM model in relation to the tip radius. At zero temperature, we have

$$\mathbf{j}(\mathbf{r}) = \int_{E_F - V_b}^{E_F} dE \int_{k_z > 0} d\hat{\mathbf{k}} \cdot \mathbf{j}_k(\mathbf{r}) , \qquad (12)$$

where V_b is the forward bias, $\hat{\mathbf{k}} = \mathbf{k}/k$ is the unit wave vector of the incident plane wave of energy, E and where

$$\mathbf{j}_k(\mathbf{r}) = \frac{\hbar}{2mi}[\psi_k^*(\mathbf{r})\nabla\psi_k(\mathbf{r}) - \psi_k(\mathbf{r})\nabla\psi_k^*(\mathbf{r})] \qquad (13)$$

is the current density carried by the scattered state $| \psi_k \rangle$. The $\mathbf{k}$ integration is over all incident ($k_z > 0$) directions. ψ_k is given by the $\mathbf{r}$ representation of Eqs. (10) and (11), namely
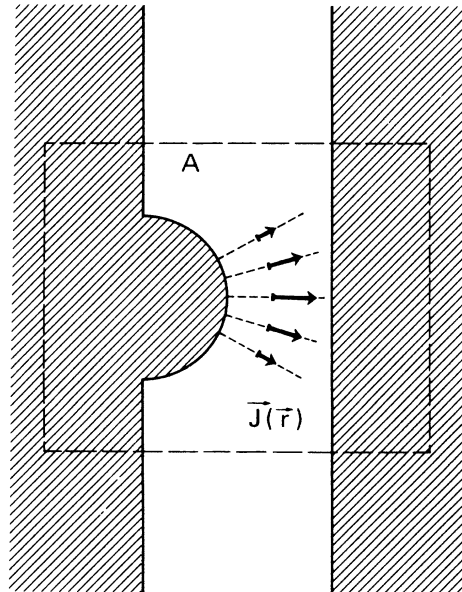
FIG. 3. Schematic illustration of the expected tunnel current density in the gap region close to the tip. The area A represents the region of space where the localized barrier associated with the boss perturbation does not vanish.

$$\psi_k(\mathbf{r})=\phi_k(\mathbf{r})+\int d\mathbf{r}' G(\mathbf{r},\mathbf{r}')V_{\text{loc}}(\mathbf{r}')\phi_k(\mathbf{r}') \ , \qquad (14)$$

$$G(\mathbf{r},\mathbf{r}')=\int d\mathbf{r}''(1-gV_{\text{loc}})_{\mathbf{r},\mathbf{r}'}^{-1}g(\mathbf{r}'',\mathbf{r}') \ . \qquad (15)$$

We intend to discretize these integral equations over a grid covering a region of space including the boss. The numerical feasibility of this discretization hinges on the crucial observation that in Eq. (14) both $\mathbf{r}$ and $\mathbf{r}'$ are restricted to lie within some close neighborhood A of the boss (Fig. 3): $\mathbf{r}$ because we want $\mathbf{j}(\mathbf{r})$ in the enclosure A and $\mathbf{r}'$ because $V_{\text{loc}}(\mathbf{r}')$, by definition, vanishes outside A. Hence we need only evaluate a finite number of matrix elements of $G(\mathbf{r},\mathbf{r}')$ from Eq. (15). It is then an easily demonstrated fact that because of the localization of V_{loc} the only matrix elements $g(\mathbf{r},\mathbf{r}')$ required to perform the indicated matrix inversion in Eq. (15) are the finite set for which both $\mathbf{r}$ and $\mathbf{r}'$ belong to A.

IV. DISCRETIZATION SCHEME

The localized property of the interesting part, V_{loc}, of the tunneling barrier allows us to cast the entire scattering problem in the form of matrix equations over a finite set of grid points. Numbering these points by the integer label i according to some convenient raster, we can write Eqs. (14) and (15) as (dropping the wave-vector index and writing V for short of V_{loc})

$$\psi_i=\phi_i+\sum_j G_{ij}V_j w_j \phi_i \ , \qquad (16)$$

$$G_{ij}=\sum_k (1-gV)_{ik}^{-1}w_k g_{kj} \ , \qquad (17)$$

where the w_j are weights characteristic of the numerical integration method (trapezoidal, Simpson, Gaussian, etc.) used to discretize the integrals.

An apparent difficulty with Eqs. (16) and (17) arises from the fact that all Green's matrices have divergent diagonal matrix elements. Indeed, in the general Green's equation

$$\left[-\frac{\hbar^2}{2m}\Delta-[E-V(\mathbf{r})]\right]G(\mathbf{r},\mathbf{r}')=-\delta(\mathbf{r}-\mathbf{r}') \ , \qquad (18)$$

the δ function is brought about by the Laplacian acting on the limiting singular behavior of G,

$$\lim_{\mathbf{r}'\to\mathbf{r}} G(\mathbf{r},\mathbf{r}')=-\frac{1}{4\pi|\mathbf{r}-\mathbf{r}'|} \ . \qquad (19)$$

However, by inspection of, e.g., Eq. (14), we see that this divergence is, in fact, canceled by the Jacobian or phase-space factor in the $\mathbf{r}'$ integration (i.e., $|\mathbf{r}-\mathbf{r}'|^2$ in spherical coordinates centered at $\mathbf{r}$). As a zeroth approximation, we are therefore entitled to exclude the diagonal term in the summations of Eqs. (16) and (17). In doing so, we neglect altogether the finite contribution of the entire "diagonal" cell $j=i$ at each computed grid point i.

While this approximation becomes exact in the limit of very small grid spacing, it may be desirable to improve on it when using the coarser grids imposed by limitations of realistic computing time and storage. Such an improvement can indeed be achieved by exploiting the known

form (19) of the Green's-function singularity. The detailed procedure is shown in the Appendix. The result, valid to order Δ^2 in the linear spacing Δ of the grid (chosen here to be simple cubic), is

$$\psi_i=(1-\tfrac{1}{2}\eta^2 V_i)\phi_i+\sum_j' G_{ij}V_j w_j \phi_j \ , \qquad (20)$$

$$\begin{aligned} G_{ij}=&[1-\tfrac{1}{2}\eta^2(V_i+V_j)][(1-\bar{g}V)^{-1}g]_{ij} \\ &-\tfrac{1}{2}\eta^2[(1-\bar{g}V)^{-1}\bar{g}V^2(1-\bar{g}V)^{-1}g]_{ij} \ , \end{aligned} \qquad (21)$$

where

$$\frac{4\pi}{3}\eta^3=\Delta^3 \ , \qquad (22)$$

and where the modified Green's matrix

$$\bar{g}_{ij}=(g_{ij}-g_{ii}\delta_{ij})w_j \qquad (23)$$

has zero diagonal matrix elements and incorporates the weight factors. Note that those results are exact in the perturbation sense, i.e., they regroup in closed form the Δ^2 corrections of all orders of perturbation in the Born series expansion of the Dyson equation (15).

V. PLANAR BARRIER TUNNELING

We need to solve the tunneling problem for the planar barrier $V_p(z)$ alone, in order to construct the Green's function $g(\mathbf{r},\mathbf{r}')$ needed for the full 3D problem. This can be done in two ways: (1) by solving the Schrödinger equation, or (2) by using the Dyson equation again.

A. Schrödinger-equation approach

In the first method, g is constructed from the wave functions of the effectively 1D Schrödinger equation for the potential $V_p(z)$. Due to the translational invariance in the $\rho=(x,y)$ directions of the planar junction, we can write the wave functions as

$$\phi(\mathbf{r})=e^{i\mathbf{k}_\parallel\cdot\rho}\phi_{k_\parallel}(z) \ , \qquad (24)$$

where $\mathbf{k}_\parallel$ is the wave vector parallel to the surface. The state satisfies ($\hbar^2/2m=1$)

$$\left[\frac{d^2}{dz^2}+\alpha-V_p(z)\right]\phi_{k_\parallel}(z)=0 \ , \qquad (25)$$

where $\alpha=E-k_\parallel^2$ is the "normal" tunneling energy. Also, the Green's function can be Fourier-analyzed according to

$$\begin{aligned} g(\mathbf{r},\mathbf{r}';\alpha)=&g(\rho-\rho',z,z';\alpha) \\ =&(2\pi)^{-2}\int d^2k_\parallel g(z,z';\alpha)e^{-\mathbf{k}_\parallel\cdot(\rho-\rho')} \ , \end{aligned} \qquad (26)$$

and the Fourier components satisfy a Green's function equation

$$\left[\frac{d^2}{dz^2}+\alpha-V_p(z)\right]g(z,z';\alpha)=\delta(z-z') \ . \qquad (27)$$

Let $\phi_1(z)$, $\phi_2(z)$ be the two independent solutions of Eq. (25) that have the following boundary conditions:

$$\phi_1(z) = \begin{cases} e^{-i\alpha_1 z}, & z \to -\infty \\ A_1 e^{i\alpha_2 z} + B_1 e^{-i\alpha_2 z}, & z \to +\infty \end{cases} \tag{28}$$

$$\phi_2(z) = \begin{cases} A_2 e^{i\alpha_1 z} + B_2 e^{-i\alpha_1 z}, & z \to -\infty \\ e^{i\alpha_2 z}, & z \to +\infty \end{cases} \tag{29}$$

where

$$\begin{aligned} \alpha_1 &= (E - k_\parallel^2 - V_{in})^{1/2}, \\ \alpha_2 &= [E - k_\parallel^2 - (V_{in} - V_b)]^{1/2} \end{aligned} \tag{30}$$

are the left- and right-hand wave vectors in the interior metal regions and where the A's and B's are incoming and reflected amplitudes. Then, it is easily verified that the Green's function is given everywhere by

$$g(z,z';\alpha) = \frac{\phi_1(z_<)\phi_2(z_>)}{W}, \tag{31}$$

where $z_<$ ($z_>$) is the smaller (the larger) of z,z' and where $W = \phi_1(z)\phi_2'(z) - \phi_2(z)\phi_1'(z)$ is the constant Wronskian of the two solutions.

The wave functions ϕ_1, ϕ_2 have been calculated using the efficient continued-fraction algorithm developed by Vigneron and Lambin[14] for the one-dimensional Schrödinger problems. Note that the wave function $\phi_2(z)$ (normalized to unit incoming flux: $A_2 = 1$) is also needed to implement the Lippmann-Schwinger equation (14) or its discretized form (20) since ϕ_2 satisfies the proper boundary condition in forward bias.

Once $g(z,z';\alpha)$ is calculated from Eq. (31), it must be Fourier-transformed in Eq. (26). Since α depends only on $k_\parallel$, the $\mathbf{k}_\parallel$ integration reduces to a single quadrature:

$$g(\mathbf{r},\mathbf{r}';\alpha) = \frac{1}{2\pi} \int_0^\infty dk_\parallel k_\parallel J_0(k_\parallel |\boldsymbol{\rho} - \boldsymbol{\rho}'|) g(z,z';\alpha). \tag{32}$$

When computing this integral, convergence difficulties are encountered at large $k_\parallel$ for the "z-diagonal" matrix elements (i.e., for $z = z'$). This is caused by the oscillatory behavior and slow decay rate of the Bessel function $J_0(x)$ for large x. A scheme to accelerate this convergence must be introduced. It is based on the physical property of g that it should tend towards the free-electron g at large $k_\parallel$. This property can be checked by inspection of the Green's equation (27) which, for large $k_\parallel$, has the solution $-\exp(-k_\parallel |z - z'|)/2k_\parallel$. Equation (32) can then be rewritten as

$$g(\mathbf{r},\mathbf{r}';\alpha) = g_f(\mathbf{r},\mathbf{r}';\alpha) + \frac{1}{2\pi} \int dk_\parallel k_\parallel J_0(k_\parallel |\boldsymbol{\rho} - \boldsymbol{\rho}'|) \left[g(z,z';\alpha) - \frac{e^{-q|z-z'|}}{-2q} \right], \tag{33}$$

where the free-electron Green's function g_f has been added and subtracted and where[15] $q^2 = k_\parallel^2 - (E - V_{in})$. Indeed, it is straightforward to check, by contour integration, that the free-electron g of energy E,

$$g_f(\mathbf{r},\mathbf{r}';\alpha) = -\frac{e^{iq_0|\mathbf{r}-\mathbf{r}'|}}{4\pi|\mathbf{r}-\mathbf{r}'|}, \tag{34}$$

where $q_0 = (E - V_{in})^{1/2}$ is the wave vector in the constant inner potential V_{in},[15] has the Fourier transform indicated as the subtracted term in the large parentheses of Eq. (33). This subtraction scheme has been found to guarantee adequate computational convergence of the integral.

B. Dyson-equation approach

In this approach, g is constructed from the Dyson integral equation exploiting the localized nature of the planar barrier in z space. Indeed, $V_p(z)$ can be split into a step potential V_{step} plus a part localized in the junction region $V_{loc}(z)$:

$$V_p(z) = V_{step}(z) + V_{loc}(z), \tag{35}$$

where

$$V_{step}(z) = \begin{cases} V_{in}, & z \le 0 \\ V_{in} - V_b, & z > 0 \end{cases} \tag{36}$$

and

$$V_{loc}(z) = V_{im}(z) - V_b(z - D)/D, \quad 0 < z < D. \tag{37}$$

The 1D Green's function $g(z,z';\alpha)$ can now be constructed from the suitably discretized Dyson equation

$$g(z,z';\alpha) = \int dz'' (1 - g_s V_{loc})^{-1}_{z,z''} g_s(z'',z';\alpha), \tag{38}$$

where $V_{loc}(z)$ is given in Eq. (37) and where g_s is the Green's function appropriate to the step barrier (36), namely

$$g_s(z,z';\alpha) = \frac{\Phi_1(z_<)\Phi_2(z_>)}{i\alpha_1\alpha_2(\alpha_1 + \alpha_2)}, \tag{39}$$

where

$$\Phi_1(z) = \begin{cases} \alpha_2 e^{-i\alpha_1 z}, & z < 0 \\ \alpha_2 \cos(\alpha_2 z) - i\alpha_1 \sin(\alpha_1 z), & z > 0 \end{cases} \tag{40}$$

and

$$\Phi_2(z)=\begin{cases}\alpha_1\cos(\alpha_1z)+i\alpha_2\sin(\alpha_1z), & z<0 \\ \alpha_1e^{i\alpha_2z}, & z>0\end{cases} \qquad (41)$$

are the two solutions of the Schrödinger equation for the step potential and where α_1,α_2 are given in Eq. (30). With $g(z,z';\alpha)$ available from Eq. (38), one can then construct the 1D wave functions $\phi_1(z),\phi_2(z)$ of $V_p(z)$ through the Lippmann-Schwinger equation

$$\phi_i(z)=\Phi_i(z)+\int_{-\infty}^{+\infty}dz'g(z,z';\alpha)V_{\text{loc}}(z')\Phi_i(z') \qquad (42)$$

discretized on the same grid as Eq. (38).

It has been found in a few test cases that the 1D Green's functions $g(z,z';\alpha)$ as calculated from Eqs. (31) and (38) agree within 1% of each other as long as a sufficiently fine grid on the z axis (100 sample points) is used to discretize Eq. (38). Which method is more efficient is a matter of the speed and accuracy of the matrix inversion and quadrature routines used to solve Eq. (38) compared to the Schrödinger integration algorithm used to solve Eq. (31). This question has not been investigated in depth, as we have chosen to use the latter method for our final numerical runs.

VI. AXIALLY SYMMETRICAL BARRIERS

The computational scheme described in Secs. IV and V is applicable to general localized 3D perturbations. However, one rapidly reaches the limits of realistic computing time and storage with relatively few sampling points in each of the three directions of space when no reduction of the size of the Green's matrices (whose dimension is equal to the number of grid points) is possible through the exploitation of some spatial symmetry of the local barrier. Twenty grid spacings in all three directions may be an upper limit with present generation computers, but this limitation is likely to be lifted in the near future with the development of more powerful machines.

Fortunately, many tunneling problems of practical interest do allow a reduction from three to two dimensions as a result of the axial symmetry of the tunneling barrier, as in the case for our model STM junction of Fig. 2. This greatly improves the possibility of reaching satisfactory accuracy in the discretization scheme with a reasonable number of grid points. We will now present the derivation of this reduction.

A. 2D Dyson equation

We start by expanding the planar wave function in Eq. (24) in Fourier series:

$$\phi(\rho,z)=\sum_{m=-\infty}^{+\infty}e^{im\phi_\rho}\phi_m(z,\rho) , \qquad (43)$$

where $\mathbf{r}=(z,\rho,\phi_\rho)$ are the cylindrical-coordinate components of $\mathbf{r}$. The Fourier components are easily ob-

tained by inverting (43) and using (24):

$$\phi_m(z,\rho)=(2\pi)^{-1}\int_{-\pi}^{+\pi}d\phi_\rho e^{ik_\|\rho\cos\phi_{k\rho}}e^{im\phi_\rho}\phi(z) , \qquad (44)$$

where

$$\phi_{k\rho}=\phi_\rho-\phi_k . \qquad (45)$$

Hence,

$$\phi_m(z,\rho)=e^{im\phi_k}J_m(k_\|\rho)\phi(z) , \qquad (46)$$

where J_m is the cylindrical Bessel function of order m. Consider now the planar Green's function g in Eq. (32); its rotational invariance is apparent through the dependence on $|\rho-\rho'|$ of the argument of J_0. Hence it has a Fourier-series representation

$$g(\mathbf{r},\mathbf{r}')=\sum_m e^{im(\phi_\rho-\phi_\rho')}g_m(z,\rho;z',\rho') . \qquad (47)$$

The coefficients g_m could be obtained via the spectral representation and the explicit form (46) of the wave functions, but it is simpler to substitute for J_0 in Eq. (32) its expansion in terms of the J_m's as given by Neumann's addition theorem[16]

$$J_0(k_\||\rho-\rho'|)=\sum_m J_m(k_\|\rho)J_m(k_\|\rho')e^{im(\phi_\rho-\phi_\rho')} . \qquad (48)$$

The result is

$$g_m(z,\rho;z',\rho')=(2\pi)^{-1}\int_0^\infty dk_\| k_\| J_m(k_\|\rho)J_m(k_\|\rho')$$
$$\times g(z,z';\alpha) . \qquad (49)$$

The full wave function and the full Green's function must also have a Fourier-series representation,

$$\psi(\mathbf{r})=\sum_m e^{im\phi_\rho}\Phi_m(z,\rho) , \qquad (50)$$

$$G(\mathbf{r},\mathbf{r}';E)=\sum_m e^{im(\phi_\rho-\phi_\rho')}G_m(z,\rho;z',\rho') , \qquad (51)$$

by virtue of the axial symmetry. It is now easy to demonstrate that the Fourier components of the wave and Green's functions for each m are related to each other by separate Lippmann-Schwinger and Dyson equations. For example, starting from

$$G(\mathbf{r},\mathbf{r}')=g(\mathbf{r},\mathbf{r}')+\int d\mathbf{r}_1 g(\mathbf{r},\mathbf{r}_1)V(\mathbf{r}_1)g(\mathbf{r}_1,\mathbf{r}')+\cdots , \qquad (52)$$

in which we introduce the expansion (47) for g and noting that $V(\mathbf{r}_1)=V(z_1,\rho_1)$ is independent of ϕ_1, we find angular integrations such as

$$\int_{-\pi}^{+\pi}d\phi_1 e^{i(m'-m)\phi_1}=2\pi\delta_{m,m'} , \qquad (53)$$

which eliminate cross terms $m\neq m'$ in all orders of the Born series. Thus, there is a separate Born series for each m component of the Green's functions in the (z,ρ) plane:

$$G_m(z,\rho;z',\rho')=g_m(z,\rho;z',\rho')+\int_0^\infty 2\pi\rho_1 d\rho_1\int_{-\infty}^{+\infty}dz_1 g_m(z,\rho;z_1,\rho_1)V(z_1,\rho_1)g_m(z_1,\rho_1;z',\rho')+\cdots . \qquad (54)$$

Using the notations

$$\mathbf{x} = (z, \rho) \ ,$$

$$\bar{g}_m(\mathbf{x}, \mathbf{x}'; \alpha) = g_m(\mathbf{x}, \mathbf{x}'; \alpha) 2\pi\rho' \ , \qquad (55)$$

we finally obtain the 2D Lippmann-Schwinger equation,

$$\Phi_m(\mathbf{x}) = \phi_m(\mathbf{x}) + \int d\mathbf{x}' G_m(\mathbf{x}, \mathbf{x}') V(\mathbf{x}') \rho_m(\mathbf{x}') \ , \qquad (56)$$

and the 2D Dyson equation

$$G_m(\mathbf{x}, \mathbf{x}') = \int d\mathbf{x}_1 (1 - \bar{g}_m V)_{\mathbf{x}, \mathbf{x}_1}^{-1} g_m(\mathbf{x}_1, \mathbf{x}') \ . \qquad (57)$$

The actual computation of g_m demands that the $\mathbf{k}_\parallel$ integration in Eq. (49) be accelerated by the add-subtract procedure of Eq. (33), the m component of which is given by

$$g_m(\mathbf{x}, \mathbf{x}') = g_m^f(\mathbf{x}, \mathbf{x}') + (2\pi)^{-1} \int_0^\infty dk_\parallel k_\parallel J_m(k_\parallel \rho) J_m(k_\parallel \rho') \left[g(z, z') - \frac{e^{-q|z - z'|}}{-2q} \right] \ . \qquad (58)$$

$g_m^f(\mathbf{x}, \mathbf{x}')$ is the m component of the free Green's function given by

$$g_m^f = -(2\pi)^{-2} \int_0^\pi d\phi \cos(m\phi) \frac{e^{iq_0(a - b\cos\phi)^{1/2}}}{(a - b\cos\phi)^{1/2}} \ , \qquad (59)$$

where

$$a = \rho^2 + \rho'^2 + (z - z')^2, \quad b = 2\rho\rho' \ . \qquad (60)$$

Note that, for computational efficiency, it is preferable to use the direct inversion of Eq. (34) to write the m component of g_f in Eq. (59) rather than its representation in terms of Bessel functions [i.e., the subtracted term in (58)]. This is because the integral in Eq. (59) is well behaved for all matrix elements, except the singular diagonal ones (at $\mathbf{x} = \mathbf{x}'$ or $a = b$), which are not required, whereas the expression in terms of the Bessel functions converges too slowly for the "z-diagonal" terms ($z = z'$).

Going from three to two dimensions weakens, but does not remove, the singularity of the diagonal matrix elements of the Green's functions. Indeed, we can write in Eq. (59)

$$\lim_{a \to 0} \int_0^\pi d\phi \cos(m\phi) \frac{e^{iq_0(a - b\cos\phi)^{1/2}}}{(a - b\cos\phi)^{1/2}}$$

$$\sim \lim_{a \to 0} \int_0^\pi d\phi \frac{1}{(a - b\cos\phi)^{1/2}} \ , \qquad (61)$$

since the singularity arises from the neighborhood of $\phi = 0$. This is the complete elliptic integral of the first kind which behaves like[17]

$$\lim_{a \to b \to 2\rho^2} \int_0^\pi d\phi \frac{1}{(a - b\cos\phi)^{1/2}}$$

$$= \frac{-2}{(a + b)^{1/2}} \ln\left[\frac{(a - b)^{1/2}}{8\rho} \right] \ , \qquad (62)$$

from which we finally get the logarithmic singularity of the Green's function,

$$\lim_{\varepsilon \to 0} g_m^f(\mathbf{x}, \mathbf{x} + \varepsilon) = \frac{1}{4\pi^2\rho} \ln\left[\frac{|\varepsilon|}{8\rho} \right] \ . \qquad (63)$$

This behavior also characterizes the planar or full Green's functions. It can be exploited to correct for the error of ignoring the diagonal cells in the discretization of Eqs. (56) and (57). The result, demonstrated in the Appendix, is

$$\Phi_m(\mathbf{x}) = [1 - s^2(\rho) V(\mathbf{x})] \phi_m(\mathbf{x}) + \sum_{\mathbf{x}_1}' (G_m V \phi_m)_{\mathbf{x}, \mathbf{x}_1} \ , \qquad (64)$$

$$G_m(\mathbf{x}, \mathbf{x}') = \{1 - [s^2(\rho) V(\mathbf{x}) + s^2(\rho') V(\mathbf{x}')]\} [(1 - \bar{g}_m V)^{-1} g_m]_{\mathbf{x}, \mathbf{x}'} - [(1 - \bar{g}_m V)^{-1} \bar{g}_m s^2 V^2 (1 - \bar{g}_m V)^{-1} g]_{\mathbf{x}, \mathbf{x}'} \ , \qquad (65)$$

where

$$s^2(\rho) = \tfrac{1}{4}\eta^2 \left[1 - \ln\left[\frac{\eta^2}{64\rho^2} \right] \right] \ , \qquad (66)$$

$$\pi\eta^2 = \Delta^2 \ , \qquad (67)$$

Δ being the spacing of the square 2D grid. In Eq. (65),

$$\bar{g}_m(i, j) = [g_m(i, j) - g(i, j)\delta_{ij}] 2\pi\rho_j w_j \qquad (68)$$

has zero diagonal elements and incorporates the integration weights w_j.

B. 2D tunnel current

In Eq. (12) for the total current density, the integration over all incident planewaves of energy E and unit wave vector $\hat{\mathbf{k}}$ amounts to a 2D integration over a semicircle of radius q_0 in the $\mathbf{k}_\parallel$ plane. Introducing then the Fourier-

series representation (50) of the full wave function, we note that there is an overall phase factor $\exp(i\phi_k)$ in each of the m components Φ_m, due to the form (46) of the planar wave functions. Hence, the angular part of the $\mathbf{k}_\parallel$ integration (over the angle ϕ_k) in the expression for the current density eliminates all cross terms with $m \neq m'$; the result is proportional to

$$\mathbf{j}(\mathbf{r}) = \int_{E_F - V_p}^{E_F} dE \int_0^{q_0} dk_\parallel k_\parallel \sum_m \mathbf{j}_m(\mathbf{r}) \ . \tag{69}$$

This expresses the fact that each m component of the wave function contributes independently to the tunneling and gives rise to additive contributions

$$\mathbf{j}_m(\mathbf{r}) = \frac{\hbar}{2mi}(\Phi_m^* \nabla \Phi_m - \Phi_m \nabla \Phi_m^*) \tag{70}$$

to the total current. Writing the gradient operator in (70) and the current $\mathbf{j} = (j_z, j_\rho, j_\phi)$ in cylindrical coordinates, one can show that there is no net j_ϕ component in the total current as a result of the cancellation of the m and $-m$ contributions. This comes from the easily verified property of the wave functions,

$$\phi_{-m}(\mathbf{x}) = (-1)^m \phi_m^*(\mathbf{x}) \ , \tag{71}$$

$$\Phi_{-m}(\mathbf{x}) = (-1)^m \Phi_m^*(\mathbf{x}) \ , \tag{72}$$

and the corresponding symmetry property of the Green's functions,

$$g_{-m}(\mathbf{x},\mathbf{x}') = g_m(\mathbf{x},\mathbf{x}') \ , \tag{73}$$

$$G_{-m}(\mathbf{x},\mathbf{x}') = G_m(\mathbf{x},\mathbf{x}') \ , \tag{74}$$

which follow from Eqs. (56) and (57) and from the fact that $J_{-m} = (-1)^m J_m$.[16] Hence we obtain, as a final formula for the 2D current density, valid for $V_b \ll E_F$,

$$\mathbf{j}(\mathbf{x}) = \frac{\hbar}{m} V_b \sum_m \int_0^{k_F} dk_\parallel k_\parallel \mathrm{Im} \left[\Phi_m^*(\mathbf{x}) \begin{pmatrix} \partial_z \\ \partial_\rho \end{pmatrix} \Phi_m(\mathbf{x}) \right] \ , \tag{75}$$

where $(\partial_z, \partial_\rho)$ is the gradient operator in the (z,ρ) plane.

Note that, without the boss, the planar MVM current $\mathbf{j}_p$ has no j_ρ component and reduces to

$$j_{pz} = \frac{\hbar}{mi} V_b \int_0^{k_F} dk_\parallel k_\parallel [\phi^*(z)\partial_z\phi(z) - \phi(z)\partial_z\phi^*(z)] \tag{76}$$

as a result of the addition property of Bessel functions:[16]

$$\sum_m J_m^2(k_\parallel \rho) = 1 \ . \tag{77}$$

The integral can be calculated at any value of z in the barrier, e.g., at $z = D$, where

$$\phi(z) = T(\alpha)e^{i\alpha z} \ , \tag{78}$$

in which $\alpha^2 = k_F^2 - k_\parallel^2$. $T(\alpha)$ is the transmission amplitude for a wave of unit amplitude incident onto the barrier. Hence,

$$j_{pz} = \frac{\hbar}{m} V_0 \int_0^{k_F} \alpha^2 |T(\alpha)|^2 d\alpha \ , \tag{79}$$

and this can serve as a reference current density to which to compare the actual distribution through the boss as computed from (75).

VII. RESULTS

As a first and simple illustration of the method, we have assumed vanishingly small forward bias and zero temperature, which allows us to confine the tunneling calculation at the Fermi level in the forward direction (tip to surface). The calculational steps proceed as follows:

(1) Construct the 3D barrier for a set of geometrical and material parameters (see Fig. 2).

(2) Choose a square grid to sample the localized barrier (we used a 9×9 grid).

(3) For a few values of the angular momentum m (we used $m = 0$–10), compute the planar wave functions from which the elements of the planar Green's matrix of Eq. (58) are calculated at the grid points.

(4) Solve for the Dyson equation (57); then solve the Lippman-Schwinger equation (56) at the grid points for enough values of the $k_\parallel$ wave vector to allow integration over $k_\parallel$ in Eq. (75).

(5) Estimate the wave-function derivatives in Eq. (75) via differentiation of a smooth parabolic interpolation between three successive grid points in each direction.

The method yields a map of (j_z, j_ρ) at all grid points. The grid chosen for this first test calculation was too coarse to obtain accurate derivatives in Eq. (75) in those regions where the wave functions vary substantially. As shown in Fig. 4, which is a 3D map of $|\Phi_m(\mathbf{x})|^2$ for $m = 0$ and $k_\parallel = 0$, there are strong accumulations and variations of amplitudes inside the boss as a result of the focusing effect of its concave surface for incoming waves. We have therefore restricted the calculation of $\mathbf{j}$ to regions where Φ_m is more slowly varying, such as along the planar surface facing the boss, which is also where we are most interested in discussing the lateral spread of the current. The results are shown in Figs. 5 and 6. The complete range of radial distances from the tip axis shown on these figures represents 5 Å, i.e., a length equal to the planar gap width D. The tip radius R was 3 Å. The tunneling is dominated by the $m = 0$ cyclindrical waves. The $m = \pm 1$ contribution to j_z peaks at less than 7% of the maximum value of the $m = 0$ term. The total j_z current carried by all waves with $|m| > 0$ amounts to less than 10% of the $m = 0$ current. In this region of the tunneling junction, the j_ρ component remains everywhere small (at most 5%) as compared to the j_z current on the axis. In general, the contribution of successive m waves to the current peaks farther away from the axis with increasing $|m|$, as one should expect from the radial dependence of the incident cylindrical wave functions. [In fact, the $m = 0$ wave is the only one to have a nonvanishing incident amplitude on the z axis; see Eq. (46)]. Turning to the principal tunneling component j_z, $m = 0$, at a radial distance from the tip axis equal to the tip ra-
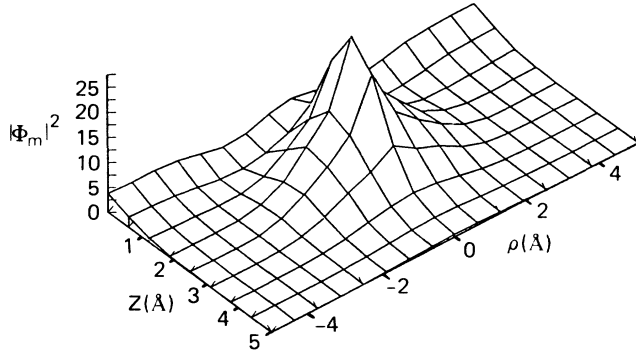
FIG. 4. Square amplitude of the wave function $|\Phi_m(\mathbf{x})|^2$ for $m = 0$ and $k_\parallel = 0$ at the grid points. The front line runs along the planar electrode. Note the accumulation of amplitude in the boss region.
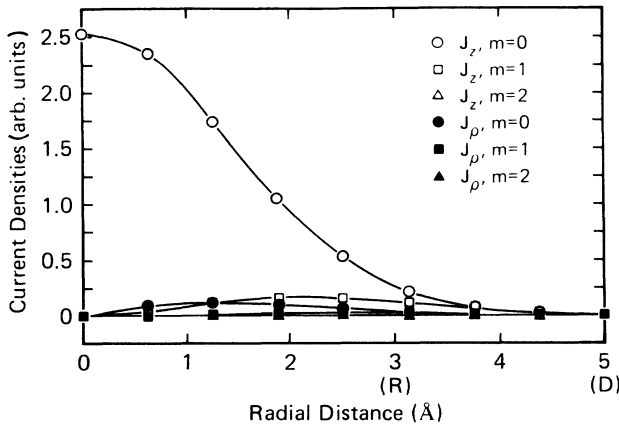
FIG. 5. Components of the tunnel current density as a function of the radial distance from the tip axis along the surface of the planar electrode. The tip radius was 3 Å. The contributions to the currents are shown for three values of the axial angular momentum m. A continuous curve has been passed through the grid-point results. The planar MVM current j_{pz} has not been subtracted because it is too insignificant on the present scale. It can be estimated from the plots on the expanded scale in Fig. 6.
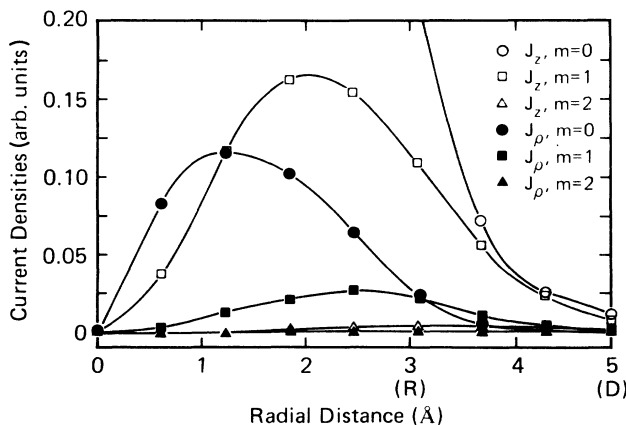
FIG. 6. Same as for Fig. 5 on an expanded current scale. Note that j_{pz} can be estimated from the asymptotic value of $j_{z,m=0}$ at $\rho = 5$. $j_{pz} \lesssim 0.01$, compared to $j_z(\rho = 0) = 2.5$.

dius the current has fallen to 10% of its value on the axis. In the present model geometry, this means that variations of barrier width or height occurring on a lateral scale of the order of the tip radius as a result of atomic corrugation of the planar surface would be easily detected. Hence our first-principles calculation confirms the fact that the lateral resolution of STM has its root in the sharp anisotropy of the tunneling phenomenon in the presence of a 3D inhomogeneous barrier.[10]

We are aware of the unrealistically small tip-to-surface distance used in our first calculation ($D - R = 2$ Å) as compared to estimated gap widths in the actual junctions (5 Å or more). The reason was that we wanted to use a coarse grid for getting numerical estimates in short computer times and this, in turn, forced us to a rather tight geometry in order for the wave functions at the Fermi level (Fermi wavelength of order 4 Å in our model) not to have too many oscillations over the tip region which is sampled by our grid. Numerical work in progress will remedy these shortcomings and also examine a range of ratios between tip radius and gap width so as to estimate the dependence of the lateral resolution on this parameter. Also, the simplifications of using zero temperature and zero bias will be removed so as to study the role of tunneling away from the Fermi surface and, particularly, the geometrical and thermal asymmetry of the tunneling current for backward versus forward biases as predicted by simple 1D tunneling calculations.[18]

To what extent can the present method be generalized to incorporate realistic features of the atomic and electronic structures of the tip and surface? One obstacle is the dimensionality of the barrier as any consideration of atomic corrugation makes the tunneling problem fully three dimensional. In the absence of the tip, a periodic 2D corrugation representative of an assumed atomic distribution on the planar surfaces can be treated by including higher Fourier components at reciprocal-lattice vectors of the corrugation into the unperturbed wave functions. From these Bloch wave functions, a pseudoplanar Green's function can then be constructed and used as the input to the Dyson equation for treating the tip perturbation, along the lines of the present scattering theoretic approach. While the difficulty of dimensionality is likely to be rapidly overcome by the availability of more powerful computers, the real problem posed by realistic material models resides in the construction of the corresponding 3D tunneling barrier, especially its correlation part which we have represented by a simple electrostatic, multiple-image potential in the calculations of this paper. The shape of the barrier is, however, intimately linked to the electronic structure of both the tip and the surface as examined by STM. Indeed, the micrographic contrast originates from such features as the density of states of the combined tip-surface system as well as from spatial inhomogeneities of the barrier. We believe that the Green's-function approach of this paper, by eliminating the uncertainties associated with the use of approximate methods to handle the tunneling part of the calculation, will facilitate the construction of barrier models representing more realistically the atomic and electronic structures of the junction materials.

VIII. FURTHER APPLICATIONS

One systematic application of the new method will be in testing various one-electron tunneling theories as applied to one and the same tunneling barrier. For example, we consider a test of the transfer-Hamiltonian method as applied to the model STM junction of the present paper.

The transfer-Hamiltonian approach requires the knowledge of the left- and right-hand wave functions of the disconnected electrodes (i.e., removed far away from each other). The tunneling rate is then computed through a current-density expression similar to Eq. (13). Can we calculate these disconnected wave functions? The right-hand electrode alone poses no problem as the wave functions are plane waves specularly reflected and phase-shifted by the single-image potential barrier of the semi-infinite metal. On the other hand, the isolated left-hand electrode, with its hemispherical boss, constitutes a case to which our localized Green's-function technique can be readily applied to work out the wave functions: starting from the unperturbed plane waves of the flat surface, the effect of the localized boss perturbation can again be obtained to all orders of perturbation by solving the corresponding scattering-theoretic equations. Thus, the left-hand wave functions can also be calculated to the desired accuracy and, hence, the transfer-Hamiltonian current density can be computed and compared to the exact results of the present work.

Finally, we wish to conclude by pointing out that some other classes of tunneling problems are amenable to a treatment by the present method. A partial list of examples follows: field emission of electrons through adsorbates[19] or through very small, atomic-size surface protrusions; field ionization of atoms in vacuum or near a metal surface;[20] ion neutralization by electron tunneling near a solid surface;[21] broadening of quasistationary levels close to a surface in chemisorption problems;[22] resonant tunneling in *M-I-M* barriers through quasistationary levels of localized atomic impurities[1] or through small metallic clusters;[23] tunneling out of electron bubbles at the surface of liquid helium;[24] electronic interaction of vacancies or small voids in metals,[25] etc. All these physical situations have in common the fact that tunneling occurs predominantly through a very restricted region of space and that the one-electron Hamiltonian, without the localized tunneling barrier, reduces, by virtue of its symmetries, to a separable problem. This is just what is required for the applicability of our new technique based on localized Green's functions and we intend in the future to exploit the method for some of the problems listed above.

APPENDIX

In this appendix we treat the singular diagonal Green's matrix elements in Eqs. (16) and (17). Equation (14) may be rewritten as (V stands here for V_{loc})

$$\psi_k(\mathbf{r}) = \phi_k(\mathbf{r}) + \int' d\mathbf{r}_1 G(\mathbf{r},\mathbf{r}_1) V(\mathbf{r}_1)\phi_k(\mathbf{r}_1)$$
$$+ \int_S d\mathbf{r}_1 G(\mathbf{r},\mathbf{r}_1) V(\mathbf{r}_1)\phi_k(\mathbf{r}_1) , \tag{A1}$$

where $\int'$ means an integration excluding a small spherical volume S of radius η centered on $\mathbf{r}$. This radius is adjusted so that S has the volume of the cubic discretization cell, as in Eq. (22). For $\eta \to 0$, we can evaluate the $\int_S$ by using Eq. (19) and noting that V and ϕ_k are continuous functions of $\mathbf{r}$:

$$\lim_{\eta \to 0} \int_S d\mathbf{r}_1 \cdots = -\tfrac{1}{2}\eta^2 V(\mathbf{r})\phi_k(\mathbf{r}) . \tag{A2}$$

In the discretization scheme, we can incorporate this small correction into the unperturbed wave function ϕ_k: the result is then Eq. (20) in the text.

Similarly, in the Born expansion of the Dyson equation (15),

$$G(\mathbf{r},\mathbf{r}') = g(\mathbf{r},\mathbf{r}') + \int d\mathbf{r}_1 g(\mathbf{r},\mathbf{r}_1) V(\mathbf{r}_1) g(\mathbf{r}_1,\mathbf{r}') + \int d\mathbf{r}_1 g(\mathbf{r},\mathbf{r}_1) V(\mathbf{r}_1) \int d\mathbf{r}_2 g(\mathbf{r}_1,\mathbf{r}_2) V(\mathbf{r}_2) g(\mathbf{r}_2,\mathbf{r}') + \cdots , \tag{A3}$$

all integrals are given the same treatment as in Eq. (A1). We keep all terms up to order η^2. Thus the first Born approximation that we designate by I_1 can be written

$$I_1 = \int'' d\mathbf{r}_1 g(\mathbf{r},\mathbf{r}_1) V(\mathbf{r}_1) g(\mathbf{r}_1,\mathbf{r}') - \tfrac{1}{2}\eta^2 [V(\mathbf{r}) + V(\mathbf{r}')] g(\mathbf{r},\mathbf{r}') . \tag{A4}$$

The double prime on the integral sign means that we exclude two small spherical volumes around the "dangerous" points $\mathbf{r}$ and $\mathbf{r}'$. We see that the first term can now be discretized excluding the diagonal matrix elements while the second term renormalizes the unperturbed Green's matrix $g(\mathbf{r},\mathbf{r}')$:

$$I_1 = (\bar{g} V g)_{\mathbf{r},\mathbf{r}'} - \tfrac{1}{2}\eta^2 [V(\mathbf{r}) + V(\mathbf{r}')] g(\mathbf{r},\mathbf{r}') , \tag{A5}$$

in which $\bar{g}$ has no diagonal elements and incorporates the weights [see Eq. (23) in the text]. The second Born term,

designated by I_2, is

$$I_2 = \int' d\mathbf{r}_1 g(\mathbf{r},\mathbf{r}_1) V(\mathbf{r}_1) \int'' d\mathbf{r}_2 g(\mathbf{r}_1,\mathbf{r}_2) V(\mathbf{r}_2) g(\mathbf{r}_2,\mathbf{r}')$$
$$- \tfrac{1}{2}\eta^2 [V(\mathbf{r}) + V(\mathbf{r}')] \int'' d\mathbf{r}_1 g(\mathbf{r},\mathbf{r}_1) V(\mathbf{r}_1) g(\mathbf{r}_1,\mathbf{r}') - \tfrac{1}{2}\eta^2 \int'' d\mathbf{r}_1 g(\mathbf{r},\mathbf{r}_1) V^2(\mathbf{r}_1) g(\mathbf{r}_1,\mathbf{r}') \ . \tag{A6}$$

The first term can be discretized; the second term renormalizes the first in the previous order, (A5); the third term will be treated below:

$$I_1 = (\bar{g}V\bar{g}V\!g)_{\mathbf{r},\mathbf{r}'} - \tfrac{1}{2}\eta^2 [V(\mathbf{r}) + V(\mathbf{r}')](\bar{g}V\!g)_{\mathbf{r},\mathbf{r}'} - \tfrac{1}{2}\eta^2 (\bar{g}V^2\!g)_{\mathbf{r},\mathbf{r}'} \ . \tag{A7}$$

After similar contractions, the third Born term I_3 becomes:

$$I_3 = \bar{g}V\bar{g}V\bar{g}V\!g - \tfrac{1}{2}\eta^2 [V(\mathbf{r}) + V(\mathbf{r}')]\bar{g}V\bar{g}V\!g - \tfrac{1}{2}\eta^2 (\bar{g}V^2\bar{g}V + \bar{g}V\bar{g}V^2)g \ . \tag{A8}$$

Again, the first term can be discretized, the second renormalizes the first in the previous order, and the third will be collected below. Clearly, the renormalization propagates throughout the entire Born series which can therefore be resummed. The terms proportional to $V(\mathbf{r}) + V(\mathbf{r}')$ simply renormalize the original Dyson expression. The leftover terms, involving distributed V^2 factors, can also be resummed in closed form via simple algebraic manipulations which the reader will easily rediscover by expanding the inverted matrices in (A9) in powers of $\bar{g}V$. The end result is

$$G(\mathbf{r},\mathbf{r}') = \{1 - \tfrac{1}{2}\eta^2 [V(\mathbf{r}) + V(\mathbf{r}')]\} [(1 - \bar{g}V)^{-1}g]_{\mathbf{r},\mathbf{r}'} - \tfrac{1}{2}\eta^2 [(1 - \bar{g}V)^{-1}\bar{g}V^2(1 - \bar{g}V)^{-1}g]_{\mathbf{r},\mathbf{r}'} \ , \tag{A9}$$

which is Eq. (21) in the text.

The demonstration of the results in Eqs. (64) and (65) proceeds exactly along the same lines as above, except that in two dimensions we use exclusion circles (instead of spheres) around the "dangerous" points, the radius of which, η, is adjusted such that the circle area coincides with the area of the square discretization cell [Eq. (67)]. The logarithmic singularity of the 2D Green's functions in Eq. (63) allow us to evaluate the diagonal-cell contribution and involves the elementary integral

$$\int_0^\eta d\varepsilon\, \varepsilon \ln \frac{\varepsilon}{8\rho} = \tfrac{1}{4}\eta^2 \left[\ln \left| \frac{\eta^2}{64\rho^2} - 1 \right| \right] \ , \tag{A10}$$

which is the $s^2(\rho)$ convergence factor shown in Eqs. (65) and (66). Care must be taken here to incorporate the ρ dependence of s^2 into the calculation of the matrix elements of Eq. (65).

*Permanent address: University of Namur, Namur, Belgium.

[1] C. B. Duke, *Tunneling in Solids* (Academic, New York, 1969).

[2] J. R. Oppenheimer, Phys. Rev. **13**, 66 (1928).

[3] J. Bardeen, Phys. Rev. Lett. **6**, 57 (1961).

[4] For a review of this work and related publications, see T. E. Feuchtwang and P. H. Cutler, Phys. Scr. **35**, 132 (1987); C. Caroli, R. Combescot, Ph. Nozières, and D. J. Saint James, J. Phys. C **5**, 21 (1972).

[5] For a recent review of STM work, see two special issues of the IBM J. Res. Dev. **30**, 4, 5 (1986); see also Ref. 4 and P. K. Hansma and J. Tersoff, J. Appl. Phys. **61**, R1 (1987).

[6] J. Tersoff and D. R. Hamann, Phys. Rev. Lett. **50**, 1998 (1983); Phys. Rev. B **31**, 805 (1985); a recent generalization of this approach is given in C. J. Chen, Phys. Rev. Lett. (to be published), see also T. E. Feuchtwang, P. H. Cutler, and N. M. Miskovsky, Phys. Lett. **99A**, 167 (1983); N. Garcia, C. Ocal, and F. Flores, Phys. Rev. Lett. **50**, 2002 (1983).

[7] N. D. Lang, Phys. Rev. Lett. **55**, 230 (1985); **56**, 1164 (1986); Phys. Rev. B **34**, 547 (1986); A. Baratoff, Physica **127B**, 143 (1984).

[8] E. Stoll, A. Baratoff, A. Selloni, and P. Carnevali, J. Phys. C **17**, 3073 (1984).

[9] J. Callaway and A. J. Hughes, Phys. Rev. **164**, 1043 (1967); J. Bernholc, N. O. Lipari, and S. T. Pantelides, Phys. Rev. Lett. **41**, 895 (1978); Phys. Rev. B **21**, 3545 (1980); G. A. Baraff and M. Schlüter, *ibid.* **19**, 1965 (1979).

[10] A. A. Lucas, J.-P. Vigneron, J. Bono, P. H. Culter, T. E. Feuchtwang, R. H. Good, Jr., and Z. Huang, J. Phys. (Paris) Colloq. **45**, C9-125 (1984); H. Morawitz, I. P. Batra, R. Reinisch, and G. R. Henry, Surf. Sci. **180**, 333 (1987).

[11] J. Bono and R. H. Good, Jr., Surf. Sci. **151**, 543 (1985).

[12] F. Seitz, *The Modern Theory of Solids* (McGraw-Hill, New York, 1940), p. 163.

[13] M. T. Michalewicz and J. Mahanty, Phys. Lett. A **116**, 392 (1986).

[14] J. P. Vigneron and Ph. Lambin, J. Phys. A **13**, 1335 (1980); **14**, 1815 (1981); H. Q. Nguyen, P. H. Cutler, T. E. Feuchtwang, N. Miskovsky, and A. A. Lucas, Surf. Sci. **160**, 331 (1985).

[15] The bias is ignored here, but this assumption can be removed by using the electron Green's function appropriate to a potential step of height V_b, see Eq. (39).

[16] G. N. Watson, *Theory of Bessel Functions* (Cambridge University Press, Cambridge, 1922).

[17] P. F. Byrd and M. D. Friedman, *Handbook of Elliptic Integrals for Engineers and Scientists* (Springer-Verlag, Berlin, 1971).

[18] A. A. Lucas, A. Moussiaux, M. Schmeits, and P. H. Cutler, Comments. Phys. **2**, 161 (1977); P. H. Cutler, T. E. Feuchtwang, T. T. Tsong, H. Nguyen, and A. A. Lucas, Phys. Rev. B **35**, 7774 (1987).

[19] C. B. Duke and M. E. Alferieff, J. Chem. Phys. **46**, 923 (1967).

[20] E. W. Mueller and T. T. Tsong, *Field Ion Microscopy: Princi-*

ples and Applications (Elsevier, Amsterdam, 1969).

[21]H. D. Hagstrum, J. Vac. Sci. Technol. **12**, 1 (1975).

[22]D. M. Newns, Phys. Rev. **178**, 1123 (1968); J. K. Norskøv and B. I. Lundqvist, *ibid.* B **19**, 5661 (1979); N. D. Lang and A. R. Williams, *ibid.* B **18**, 616 (1978).

[23]R. W. Rendell, B. Muehlschlegel, and D. J. Scalapino, Phys. Rev. Lett. **41**, 1746 (1978); R. W. Rendell and D. J. Scalapino, Phys. Rev. B **24**, 3276 (1981).

[24]M. W. Cole and J. R. Klein, J. Low. Temp. Phys. **36**, 331 (1979).

[25]A. A. Lucas, Physica **127B**, 225 (1984).